Title	Thermal transient test and strength evaluation of a tubesheet structure made of Mod.9Cr-1Mo steel. Part ??: Creep-fatigue strength evaluation
Author(s)	Masanori Ando, Shinnichi Hasebe, Sumio Kobayashi, Naoto Kasahara, Akira Toyoshi, Takahiro Ohmae and Yasuhiro Enuma
Citation	Nuclear Engineering and Design, 275, p.422-432.
Text Version	Author
URL	http://jolissrch-inter.tokai-sc.jaea.go.jp/search/servlet/search?5042476
DOI	http://dx.doi.org/10.1016/j.nucengdes.2014.04.029
Right	NOTICE: This is the author's version of a work that was accepted for publication in Nuclear Engineering and Design. Changes resulting from the publishing process, such as peer review, editing, corrections, structural formatting, and other quality control mechanisms, may not be reflected in this document. Changes may have been made to this work since it was submitted for publication. A definitive version was subsequently published in Nuclear Engineering and Design, VOLUME 275, 2014, DOI: 10.1016/j.nucengdes.2014.04.029. c2014 Elsevier B.V. All rights reserved.©2014 Elsevier B.V. All rights reserved.

Title

Thermal transient test and strength evaluation of a tubesheet structure made of Mod.9Cr-1Mo steel. Part II: Creep-fatigue strength evaluation

Authors

Masanori Ando

Japan Atomic Energy Agency, Oarai-cho, Higashi-ibaraki, Ibaraki, 311-1393, Japan

ando.masanori@jaea.go.jp

TEL; 8129-267-4141, FAX;8129-266-3675

Shinnichi Hasebe

Japan Atomic Energy Agency, Oarai-cho, Higashi-ibaraki, Ibaraki, 311-1393, Japan

hasebe.shinnichi@jaea.go.jp

TEL; 8129-267-4141, FAX;8129-267-2397

Sumio Kobayashi

Japan Atomic Energy Agency, Oarai-cho, Higashi-ibaraki, Ibaraki, 311-1393, Japan

kobayashi.sumio@jaea.go.jp

TEL; 8129-267-4141, FAX;8129-267-2397

Naoto Kasahara

Japan Atomic Energy Agency, Oarai-cho, Higashi-ibaraki, Ibaraki, 311-1393, Japan

(Presently; The University of Tokyo /Hongo, Bunkyo-ku, Tokyo, Japan, 113-8656)

kasahara@n.t.u-tokyo.ac.jp

TEL&FAX ; 813-5841-0247

Akira Toyoshi

Mitsubishi heavy industries, Ltd, Hyogo-ku Kobe, Hyogo, 676-8585, Japan

akira_toyoshi@mhi.co.jp

TEL; 8178-672-5099, FAX ; 8178-672-3435

Takahiro Ohmae

Mitsubishi heavy industries, Ltd, Hyogo-ku Kobe, Hyogo, 676-8585, Japan

takahiro_omae@mhi.co.jp

TEL; 8178-672-3418, FAX ; 8178-672-3435

Yasuhiro Enuma
Mitsubishi FBR systems, Inc., Jingumae, Shibuya-ku, Tokyo, 150-0001, Japan
(Presently; Japan Atomic Energy Agency, Oarai-cho, Higashi-ibaraki, Ibaraki, Japan, 311-1393)
enuma.yasuhiro@jaea.go.jp
TEL; 8129-267-4141, FAX;8129-267-1676

Abstract

The tubesheet structure is one of the components that suffer the most severe loading in fast reactors, and it is one of the most difficult components to design because of such severe operation conditions and its complex three-dimensional structure with an arrangement of numerous penetration holes. In this study, the strength of a tubesheet test model simulating a semispherical tubesheet structure subjected to cyclic thermal transients was evaluated using the finite element analysis (FEA). A test model made of Mod.9Cr-1Mo steel was subjected to 1,873 cycles of severe thermal transient loading using a large-scale sodium loop, in which elevated-temperature sodium at 600°C and 250°C was flowed repeatedly and kept at the final temperature for 2 and 1 h, respectively. Heat transfer analysis and stress analysis were performed using the sodium temperature data measured during the test. The boundary conditions were adjusted to simulate the measured temperature distribution on the inner and outer surfaces of the test model in the heat transfer analysis, and the result was used for the stress analysis. Then, the elastic and inelastic stress analysis results were used to investigate the failure mechanism by creep-fatigue damage and evaluate the failure strength. The evaluation based on the results of inelastic analysis estimated the number of cycles to failure within a factor of 3 of the total number of thermal loading cycles 1,873, which corresponds to the number of cycle at which the crack reached 2.59 mm.

Keywords

Heat-resistant steel, Fatigue, Creep-fatigue interaction, Elevated temperature design

1. Introduction

Mod.9Cr-1Mo steel is a candidate material for the primary and secondary heat transport system components of the Japan sodium-cooled fast reactor (JSFR) (Aoto et al., 2011). However, there is little hard evidence to support the structural integrity of components made of Mod.9Cr-1Mo steel under actual environments. Therefore, a thermal cyclic test was performed with a tubesheet model simulating the center-flattened spherical tubesheet (CFST) (Ando et al., 2013a). The test results were summarized in the associated paper (Ando et al., 2013b), which includes the details of the tubesheet model design and the test procedure.

Since the CFST was an original design and no data validating its structural integrity are available, the main objectives of this study are to clarify the failure mode and mechanism and to validate the applicability of the strength evaluation methods for the tubesheet model. To achieve these objectives, finite element analysis (FEA) was performed using the temperature data measured during the test, and the calculated stress and/or strain data were compared to the test results to analyze the failure mode of the tubesheet model simulating the CFST structure. To validate the strength evaluation methods based on elastic and inelastic FEA, the experimentally obtained strength data reported in the associated paper (Ando et al., 2013b) were used.

The CFST was designed as the tubesheet structure of steam generator (SG) to satisfy several requirements for the SG of the JSFR (Chikazawa et al., 2012; Kurome et al., 2010; Futagami et al., 2009). In this SG, the planned pressure of the outlet steam is 19.2 MPa with temperature reaching 497°C under normal operation. Mod.9Cr-1Mo steel is planned to be adopted as the material of the SG, because this steel has both excellent thermal properties and high-temperature strength with good stress corrosion cracking resistance.

To validate the manner of failure in the originally developed CFST under cyclic thermal transients, a tubesheet model simulating the CFST was designed and a cyclic thermal loading test was performed. Since sodium has a large thermal capacity with a low pressure, the strength test was performed in a sodium environment, although the real tubesheet in the actual SG is used in a steam environment, where water flows from the lower plenum to the upper plenum through the heat exchanger tube. However, sodium flows from the upper plenum to the penetration holes of the tubesheet in this test, which makes the environment different. Nevertheless, the location of crack initiation, the distribution of cracks, and the direction of crack propagation were supposed to be simulated in the test. In fact, the stress inducement mechanism in the test model was comparable to that of the CFST, because the mechanism in the CFST under the thermal transition was analyzed and considered in the design of the test model (Ando et al., 2013a).

In the test, hot and cold sodium were supplied from the inlet nozzle and then flowed into the upper plenum with a constant rate of 100 l/min. During the hot transient, sodium heated to

600 °C was flowed into the test model, and a constant sodium flow was maintained for 2 h. During the cold transient, sodium heated to 250 °C was flowed into the test model, and a constant sodium flow was maintained for 1 h. The 2 h hold at 600 °C after the hot transient was chosen to generate creep damage due to stress relaxation. The 1 h hold at 250 °C after the cold transient was chosen to eliminate the temperature distributions in the test model and the TTS components for the following cycle. The electromagnetic pumps installed in each circuit enabled the temperature change rate of the flowing sodium to be controlled at 5 °C/s. A total of 1,873 thermal transient cycles were applied to the test model. Afterward, the test model was removed from the TTS. Then, the test model was inspected by performing liquid penetrant testing (PT) on the outer surface and cut to perform PT on the inner surface. No cracks were observed on the inner or outer side of the test model, except for on the hole edges of the tubesheet. In fact, many cracks were observed by PT on the upper surface of the tubesheet and on the inner surfaces of the penetration holes. Therefore, only the tubesheet structure was examined in this study. Details of the test model, experimental procedure and results of the PT and hardness test were summarized in the associated paper (Ando et al., 2013b).

For the creep-fatigue-life evaluation, the environmental effect of sodium was not considered in this study. According to several reports regarding Mod.9Cr-1Mo steel, its fatigue life is significantly improved in a sodium environment (Asayama et al., 2001; Kannan et al., 2009). In contrast, the creep-fatigue life is not improved in a sodium environment (Asayama et al., 2001), and the same results were obtained under high-vacuum conditions (Riou et al., 2008). Overall, these results suggest that internal creep damage becomes predominant in creep-fatigue tests. In particular, crack initiation on the surface is retarded in a sodium environment because oxidation was suppressed under an oxygen density of less than 6 ppm.

2. Thermal stress analysis

2.1 Model for the finite element analysis

Both elastic and inelastic FEAs were performed using the FINAS code (Japan Atomic Energy Agency. et al., 2008). Here, inelastic FEA means an elastic-plastic-creep FEA. The FEA model is shown in Fig. 1, and the dimensions were based on those of the test model (Ando et al., 2013b). A three-dimensional (3D) FE model with 30° sectors was used to evaluate the peak stress generated by the stress concentration around the hole edges. The 8-node quadrilateral axisymmetric elements HQAX8/QAX8 of the FINAS code were utilized for this calculation. The material properties used in the FEA were obtained from the open literature (American Society of Mechanical Engineers, 2011a; JSME, 2012), as listed in Table 1. For the inelastic analysis, the constitutive equation was utilized to be a bilinear stress-strain relationship, and the values of the proportional limit and the work hardening coefficient were obtained from the

cyclic stress-strain relationship of Mod.9Cr-1Mo steel (Ando et al., 2013c). The constitutive equation of the creep strain behavior was that in the JSME FR code (JSME, 2012).

2.2 Heat transfer analysis

Heat transfer analysis was performed using the sodium temperature data measured during the test. The temperature distribution in the test model during the test was estimated by performing heat transfer analysis using the measured sodium temperature data to provide the input data for the thermal stress analysis. The measured sodium temperature was assigned to 11 regions to simulate the temperature distribution in the test model. The relationship between the measured sodium temperature and the assigned region is shown in Fig. 2. All of the positions for the temperature measurement were reported in the associated paper (Ando et al., 2013b). The relationship between the assigned region and the sodium temperature was adjusted by checking the relationship between the results of a trial analysis and the measured temperature distribution on the surface of the test model.

In the heat transfer analysis, the boundary condition was adiabatic on the outer surface of the test model, because the test model was covered with a thermal insulator during the test. On the inner surface, which was exposed to a heat flow due to the flowing sodium, a heat transfer element was used and the coefficient was evaluated based on the Seban-Shimazaki correlation, as shown in Fig. 3.

The calculated results are shown in Fig. 4 along with the measured data from the test. It is evident that the simulation was adequate, especially for the relationship of the temperature changes. Since temperature differences in the model cause thermal stress, the relationship of the temperature changes is very important for the thermal stress analysis. In fact, the assignment of the region and adjustment of the sodium temperature was performed especially with regard to the relationship of the temperature changes. Even though only several representative data are shown in Fig. 4, the relationships between the other temperature histories measured in the test and the calculated results were also confirmed.

The temperatures distribution simulated at certain times during the hot and cold transient are shown in Fig. 5. At 182 s from the start of the hot transient, the temperatures of the upper surface of the tubesheet and the inner surfaces of the penetration holes were higher than that of the inside surface. In contrast, the temperature of the center of tubesheet was lower than that of the outer side at 110 s from the start of the cold transient.

2.3 Thermal stress analysis

The elastic and inelastic FEA were conducted using the temperature distribution data calculated in the heat transfer analysis. The defined boundary condition is shown in Fig. 6.

Identification numbers were assigned to distinguish each hole, and these are also shown in Fig. 6. A set of thermal loadings (hot and cold thermal transients) was calculated.

The elastic analysis was performed using the results of the heat transfer analysis, and the equivalent stress calculated at the elapsed times of 182 s and 110 s from the hot transient and cold transient, respectively, are shown in Fig. 7. These were the times when the maximum calculated equivalent stress was generated in each transient. Because of the differences in the temperature distributions, the location at which the large stress is generated is different for each transition.

In the hot transition, a larger stress was calculated at the edges of holes *a*, *c*, and *d* in Fig. 6. In the outermost hole *d*, this larger stress was generated at the hole edge on the center side. In contrast, a larger stress was generated at the hole edges on the both center and outer sides of holes *a* and *c*.

In the cold transient, a larger stress was also calculated at the edges of holes *a*, *c*, and *d* in Fig. 6. In holes *a* and *d*, a larger stress was generated at the hole edge in the direction connecting the hole center to that of the nearest hole. In the stress distribution around hole *c*, a larger stress was generated at the hole edge in the directions connecting holes *a* and *c* and connecting *c* and *d*. The stress level was lower in the direction connecting *c* and *g*.

In the elastic analysis, the combination of the time points that generated the maximum equivalent stress range was determined. The distribution of the calculated stress ranges was quantified, as shown in Fig. 8. To clarify the relationship between the stress ranges generated and locations, stress range was associated with the rotation angle of the holes. In all the holes, the meridian direction was aligned along φ = 0° and 180°, and 0° was defined as the outer side of the tubesheet. Figure 8(A) shows the stress range around the hole edge on the upper surface of the tubesheet. The largest stress range was calculated at 227° on the edge of hole *d*. The relationships between the stress range and the angle differ by each hole. Figure 8(B) shows the stress range along the surface of the penetration hole. It is evident that the largest stress range on these lines was generated at the upper surface of the tubesheet, except at 0° on hole *d*. In fact, the maximum stress range was calculated at 0° on the edge of hole *d* on the lower surface, although no crack was detected in this area.

In the inelastic analysis, five cycles of thermal transients were calculated, and the calculated results for the last cycle were used for the estimation of the strain ranges. For the elastic-plastic-creep constitutive equation, the kinematics hardening rule was applied. The strain ranges calculated in the inelastic analysis are shown in Fig. 9. The equivalent strain range, $\Delta\varepsilon_{\mathrm{equiv}}^{\mathrm{EP}}$, was assumed to be the sum of the elastic strain range, $\Delta\varepsilon_{\mathrm{equiv}}^{\mathrm{e}}$, and the plastic-creep strain range, $\Delta\varepsilon_{\mathrm{equiv}}^{\mathrm{in}}$, calculated using the following equations:

$$\Delta\varepsilon_{\mathrm{equiv}}^{\mathrm{e}} = \frac{\sqrt{2}}{3}\sqrt{((\Delta\varepsilon_r - \Delta\varepsilon_z)^2 + (\Delta\varepsilon_r - \Delta\varepsilon_\theta)^2 + (\Delta\varepsilon_\theta - \Delta\varepsilon_r)^2 + \frac{3}{2}\Delta\tau_{rz}{}^2)} \times \left(\frac{1.5}{1+\nu}\right) \quad (1)$$

and

$$\Delta\varepsilon_{\mathrm{equiv}}^{\mathrm{in}} = \frac{\sqrt{2}}{3}\sqrt{((\Delta\varepsilon_r - \Delta\varepsilon_z)^2 + (\Delta\varepsilon_r - \Delta\varepsilon_\theta)^2 + (\Delta\varepsilon_\theta - \Delta\varepsilon_r)^2 + \frac{3}{2}\Delta\tau_{rz}{}^2)} \quad , \quad (2)$$

where $\Delta\varepsilon_r$, $\Delta\varepsilon_z$, $\Delta\varepsilon_\theta$, and $\Delta\tau_{rz}$ indicate the radial, axial, hoop, and shear strain ranges calculated on the basis of the FEA results for the hot and cold transients, and ν is Poisson's ratio.

As in the elastic analysis, the strain range was associated with the rotation angle around the holes. Again, the relationship between the strain range and angle depends on the hole location. The maximum strain range on the upper surface was about 0.61% at the edge of hole *d*.

3. Creep-fatigue strength evaluation

3.1 Characterization of the failure

In the associated paper, it was observed that the failure mode was crack initiation at the surface of the penetration hole due to cyclic loading and propagation of these cracks in the creep-damaged area near the upper surface of the tubesheet (Ando et al., 2013b). This failure mode was supported by the fracture surface observation and hardness test. To confirm this failure mode, the FEA results were further analyzed. In particular, the relationship between the crack initiation/propagation region and the calculated stress/strain was investigated.

Because stress was generated by the thermal transient due to the flowing sodium in the tubesheet model simulating the CFST, a larger thermal stress was generated near the inner surface. Such a stress distribution caused creep damage only to the nearby surface region during the period of high temperature. The stress histories during a thermal cycle calculated in the inelastic analysis are shown in Fig. 10. In this figure, the hoop and radial stress are in the circumferential direction and meridian direction, respectively. The stress history at 227° on the edge of hole *d* on the upper surface is shown in Fig. 10(A). It is evident that the dominant stress was hoop stress, and it remained a tensile stress after the hot transient. On the other hand, Fig. 10(B) shows the stress history at 0° on the edge of hole *d* on the lower surface of the tubesheet. In fact, the maximum stain range of 0.8% was calculated in the inelastic analysis at this position, although no crack was detected after the test. The dominant stress was hoop stress in this position too, and it remained a compression stress after the hot transition. In the creep-fatigue test under the sodium environment, the compressive holding has an insignificant effect on the failure life (Asayama et al., 2001; Kannan et al., 2011). The number of cycles to failure in the creep-fatigue test with compressive holding under a sodium environment was similar to that in

the fatigue test under a sodium environment. Under the sodium environment, the number of cycles to failure in the fatigue test with a strain range $\Delta\varepsilon$ = 0.8% at 600 ºC was predicted to be more than 10,000 (Kannan et al., 2011). This clarifies that the creep effect by tension holding has a significant role in the crack initiation and propagation. The cracks were initiated and propagated only in the area having tensile stress after the hot transition, which validates that the failure mode was crack initiation on the surface of the penetration hole, very near the hole edge, due to cyclic loading and propagation of the cracks in the creep-damaged area near the upper surface of the tubesheet. It concludes as the main failure mechanism in the tubesheet structure is the crack initiation caused by creep-fatigue due to cyclic hoop stress with tension holding and crack propagation near the upper surface of the tubesheet.

Finally, the FEA result indicates that the thermal stress is larger at the surface and lower in the interior of the test model. As a result, cracks were likely to be initiated on the penetration surface very near to the upper surface and propagated in the creep-damaged area near the upper surface of the tubesheet from the hole edge to the nearest neighboring hole. These cracks then propagated to the inside of the test model, where there was less creep damage, thus causing striations. This crack propagation mechanism is similar to that of the thick cylinder model tested in parallel to this investigation (Ando et al., 2013d).

3.2 Evaluation of the creep-fatigue life based on finite element analysis

To evaluate the creep-fatigue life, the results of the elastic and inelastic analyses were used. The stress redistribution locus (SRL) method and simple elastic follow-up (SEF) method (Kasahara et al., 2001; Ando et al., 2012a) were employed using the results of the elastic analysis.

The SRL method is a simplified technique for predicting the local stress-strain behavior in a structure. This concept proposes that a certain locus of stress redistribution is available for a structure, and it can predict the relationship between the elastic-plastic-creep strain and stress from the peak stress on the surface calculated by elastic analysis. An optimized reduction factor of κ = 1.6 was used, assuming an ideal case in the SRL method.

The SEF method is also a simplified technique for predicting the local stress-strain behavior. It assumes that a certain ratio between the elastic strain gradient and the plastic strain gradient is available for the structure. As for the creep behavior, it assumes that the stress relaxation rate of the local strain/stress concentration point in the structure caused by creep phenomena can be predicted by dividing the product of the creep strain ratio and Young's modulus by the elastic coefficient q. The concept of the elastic follow-up method is incorporated into the current design and construction code for the fast reactor in Japan (JSME, 2012). In the SEF method, the elastic follow-up factor of q = 3 was used as a conservative recommended value.

To estimate the creep-fatigue life using the inelastic analysis results, the procedure summarized in Fig. 11 was applied. This procedure using the strain ranges calculated by the inelastic analysis was proposed as a simple evaluation procedure, although a direct estimation of the creep damage from the calculated stress history in the inelastic analysis could be conceived. Since it was supposed that the complex procedure would depend on the estimator and that a conventional procedure would not be available for validation, a simple procedure was applied in this study.

The number of cycles to failure around the edges of holes *a*, *c*, *d* and *g* estimated using each method are shown in Fig. 12, along with the observed cracks. The observed cracks were superimposed, since the holes were located in a geometrically similar pattern at every 30°. It is apparent that angles with less estimated failure cycles are in good agreement with the angles with longer observed cracks around holes *a* and *d*. These results indicate that a good simulation was achieved using this model and boundary condition. However, the relationship between the estimated failure cycles and the cracks was not clear around hole *c* and *g*. Around hole *c*, areas with longer cracks were in the direction of the lines connecting hole *c* and holes *a* or *g* at 286° or 106°, respectively. Similarly, around hole *g*, the cracked areas were in the direction of the lines connecting hole *g* and hole *c* or *f* at 270° or 210°, respectively. It seems that crack propagation might be involved in this relationship. The smallest number of cycles to failure was estimated for hole *d*, although the maximum crack lengths around this hole were comparable to those around holes *a* and *c*. The minimum number of cycles to failure was comparable for hole *g* to *c*, however, the number of cracks and average crack length were larger and longer for hole *c*, respectively. These results imply that crack propagation was not correlated well with the calculated stress and/or strain range. Interactions between each crack and/or hole and the stress component are likely to affect the crack propagation. The reason for a different relationship for the non-outermost hole *c* and *g* may be due to this.

The relationship of the crack length and the estimated creep-fatigue lives based on results of inelastic FEA (Fig.11) are shown in Fig. 13. In the Fig. 13, there is a distribution trend that longer crack was observed where the less life was estimated around the hole edges of *a* and *d*. It is reasonable results because the location estimated less lives initiated cracks earlier and these were propagated, although such distribution trend of hole *a* is shifted to the longer life side. It seems that there are two peaks in the relationship between crack length and the estimated lives around the edge of hole *d*, and the one of the peaks located at the longer life side corresponds to the peak of the hole *a*. Detail analysis of the FEA results clarified that the second peak, located at longer life side, in the hole *d* consist of the cracks located around the hole edge on the direction connecting holes center of *c* and *d*, and larger stress amplitude generated around such direction during both the hot and cold transient (Fig. 7). On the other hand, in the Fig. 13, the

second peak in hole *d* and the peak in hole *a* consist of the cracks located at about 130 ° (defined in Fig. 8) in both holes. At these locations, larger stress amplitude generated only during the cold transient (Fig. 7). These results may imply that stress amplitude during hot/cold transient was over/under estimated. In other word, if less/larger stress amplitude was calculated at these locations during the hot/cold transient, all peaks might be overlapped. However, further tuned heat transfer analysis to correspond the temperature distribution in FEA to that in the experimentally obtained is unpractical.

In contrast, any certain trend is not cleared in the hole *c* and *g*. This disagreement is supposed to be caused by the complex interaction of each hole to crack propagation as that of the above-mentioned.

Since this failure test was performed using a thermal transient due to flowing sodium, the severe cyclic thermal transient and the sodium environment prevented the direct acquisition of data for the specific cycles corresponding to the crack initiation and the crack propagation process. For these crack observations, only the total number of transient cycles (1,873) was known, and this total cycle includes both the crack initiation and propagation processes. Therefore, it may not be appropriate to compare this number with the evaluated number of cycles to failure determined on the basis of the FEA results. In the previous papers, a creep-fatigue life criterion for structural testing was defined as the number of cycles corresponding to a crack length on the surface that reached 1.0 mm, N_{1mm}, which was used to estimate the number of cycles to failure (Ando et al., 2011, 2012b, 2013d).

The number of cycles at which a crack reached 1.0 mm was reported to be about 70% of the number of cycles to failure in a 600 °C, $\Delta\varepsilon$ = 0.5% fatigue and creep-fatigue test performed on Mod.9Cr-1Mo steel (Miyahara et al., 1995; Ishii et al., 2000). In the results of some creep-fatigue tests at 593°C and $\Delta\varepsilon$ = 0.50% or 0.51% with 1 h of holding on the tension side, the number of cycles to failure was about 2,900 (Bernard Riou, 2008) both in air and in a high vacuum. Taking into account such reports and because the $\Delta\varepsilon$ estimated by the inelastic analysis was about 0.6% on the tubesheet surface, the observation of crack of 2.59 mm on the upper surface of the tubesheet after 1,873 loading cycles was reasonable. Therefore, the total number of testing cycles, 1,873, was assumed to be the number of cycles to failure of the test model. However, N_{1mm} was applied in the previous papers. The difficulty of assessment using the failure mechanics techniques to the hole edges of the tubesheet model discouraged the estimation of N_{1mm}.

The results for 227° on hole *d* on the upper surface, where the maximum strain range was generated in the inelastic analysis, calculated using the Campbell diagram are shown in Fig. 14. For the evaluation, 1,873 test cycles were used. For the calculation based on the inelastic analysis results, the accumulated fatigue damage factor D_f was less than 1.0, and the creep

damage factor D_c exceeded 1.0. The ratio of fatigue damage factor to creep damage factor was approximately 0.20, since D_f:D_c = 1:5. Using the SRL method and the SEF method, accumulated fatigue and creep damage factors were calculated which are comparable. In these methods, both the accumulated fatigue and creep damage factors exceeded 1.0, with ratios of fatigue damage to creep damage of approximately 0.35 (D_f:D_c = 2.2:6.3) and 0.20 (D_f:D_c = 1.4:7.1), respectively. In all the methods, creep damage factors were greater than fatigue damage factors. Figure 15 shows the relationship between the estimated number of cycles to failure at 227° on hole *d* and the total number of thermal loading cycles 1,873, which corresponds to the number of cycles at which the crack reached 2.59 mm at that location. The numbers of cycles to failure estimated using the SRL method and the SEF method were within a factor of 10 of the total number of thermal loading cycles. The estimated number of cycles to reach failure based on inelastic analysis was within a factor of 3. If the observation of 1.0 mm surface cracks was possible and N_{1mm} could be used, the predictions of these evaluation methods would be within a smaller factor of the total number of thermal loading cycles.

4. Conclusion

The result of a cyclic thermal transient test of a tubesheet model made of Mod.9Cr-1Mo steel was evaluated using FEA. To simulate the stress and strain in the complex 3D structure of the CFST, a 3D FEA model was used in the evaluation. Based on the measured temperature on the surface of the test structure and the measured sodium temperature, the thermal distribution during the test was simulated using adjusted thermal coefficients. Elastic and inelastic stress analyses were conducted using these calculated temperature distribution data. The failure mode and the evaluation of the creep-fatigue life were evaluated based on the FEA results. The results are summarized as follows:

(1) The lifetimes estimated using each method agreed well with the observed crack distributions in the outermost holes *d* and *g*.

(2) Comparison between the stress history of a hole edge on upper surface and lower surface indicated that tensile creep damage strongly accelerated the crack initiation.

(3) The evaluation based on the results of inelastic analysis estimated the number of cycles to failure within a factor of 3 of the total number of thermal loading cycles 1,873, which corresponds to the number of cycle at which the crack reached 2.59 mm at 227° on hole *d*.

(4) The SRL and SEF methods estimated the number of cycles to failure within a factor of 10 of the total number of thermal loading cycles 1,873, which corresponds to the number of cycles at which the crack reached 2.59 mm at 227° on hole *d*.

Acknowledgement

This paper includes results of the “Technical development program on a commercialized FBR plant” entrusted to the Japan Atomic Energy Agency (JAEA) by the Ministry of Economy, Trade and Industry of Japan (METI). The authors wish to express their gratitude for the enthusiastic effort in the design and fabrication of the test model by Mr. Usui and co-workers of Mitsubishi Heavy Industry, Ltd. The authors are also grateful to Mr. Osamu Inoue of IX Knowledge, Inc., for performing the FEA, evaluation and participating in useful discussions.

References

- American society of mechanical engineers(ASME), 2011a, An international code 2010 ASME Boiler & Pressure Vessel Code 2011a Addenda, Section II, Part D (Customary), Materials.
- Ando, M., Takasho, H., Kawasaki, K., Kasahara, N., 2013a, Stress mitigation design of tubesheets with consideration of thermal stress inducement mechanism, Journal of Pressure Vessel Technology, Vol.135, Issue 6, pp.061207-1-061207-10
- Ando, M., Hasebe, S., Kobayashi, S., Kasahara, N., Toyoshi, A., Ohmae, T., Enuma, Y., 2013b, Thermal transient test and strength evaluation of a tubesheet structure made of Mod.9Cr-1Mo steel. Part I : Test model design and experimental results, Journal of Nuclear Engineering and Design, to submit
- Ando, M.. Watanabe, S., Kikuchi, K., Otani, T., Satoh, K., Tsukimori, K., Asayama, T., 2013c, Development of 2012 Edition of JSME Code for Design and Construction of Fast Reactors (6)Design margin assessment for the new materials to the rules, Proceedings of ASME PVP 2013, 2013, PVP2013-97803
- Ando, M., Hirose, Y., Karato, T., Watanabe, S., Inoue, O., Kawasaki, N., Enuma, Y. 2011, Comparison of Creep-fatigue evaluation methods with notched specimens made of Mod.9Cr-1Mo steel”, Proceedings of ASME Pressure Vessel and Piping Conference 2011, PVP2011-57532, 2011
- Ando, M., Hirose, Y., Watanabe, S., Enuma, Y., Kawasaki, N., 2012a, Verification of the prediction methods of strain concentration in notched specimens made of Mod.9Cr-1Mo steel, Journal of pressure vessel and technology, Vol.134, Issue 6, pp. 061403-1 - 061403-12
- Ando, M., Kanasaki, H., Date, S., Kikuchi, K., Sato, K., Takasho, H., Tsukimori, K. 2012b, A study on fatigue and creep-fatigue life assessment using cyclic thermal tests with Mod.9Cr-1Mo steel structures, Proceedings of ASME Pressure Vessel and Piping Conference 2012, PVP2011-78042
- Ando, M., Hasebe, S., Kobayashi, S., Kasahara, N., Toyoshi, A., Ohmae, T., Enuma, Y., 2013d, Thermal transient test and strength evaluation of a thick cylinder model made of

Mod.9Cr-1Mo steel, Journal of Nuclear Engineering and Design, No.255, pp.296-309

- Aoto, K., Uto, N., Sakamoto, Y., Ito, T., Toda, M., Kotake, S. 2011. Design Study and R&D Progress on Japan Sodium-Cooled Fast Reactor. Journal of Nuclear Science and Technology 2011, Vol.48, pp.463-471
- Asayama, T., Abe, Y., Miyaji, N., Koi, M., Furukawa, T., Yoshida, E. 2001, Evaluation procedures for irradiation effects and sodium environmental effects for the structural design of Japanese fast breeder reactors, Journal of Pressure Vessel Technology, Vol.123, pp.49-57
- B., Riou, 2008, Improvement of ASME NH for Grade 91 negligible creep and creep fatigue, STP-NU-013, ASME standards technology, LLC, New York.
- Futagami, S., Hayafune, H., Fujimura, K., Sato, M., 2009, A Study on LMFBR steam generator design without tube failure propagation in water leak events, Proceedings of 2009 International Congress on Advances in Nuclear Power Plants (ICAPP '09), pp1419-1428
- Ishii, R., Kimura, K., Fujiyama, K., Hongo, S., Saito, K., 2000, Evaluation of damage for modified 9Cr-1Mo steel, Journal of high pressure institute Japan, Vol.38, pp.4-11, (Japanese)
- Japan Atomic energy agency and Itochu Techno-Solutions, 2008, FINAS User's Manual Ver.19.0, (in Japanese)
- Japan Society Mechanical Engineers(JSME), 2012, Code for Nuclear Power Generation Facilities, Rules on Design and Construction for Nuclear Power Plants, Section II Fast Reactor Standards, 2012, JSME S NC2-2012(in Japanese)
- Kannan, R., Ganesan, V., Mariappan, K., Sukumaran, G., Sandhya, R., Mathew, D., M., Rao, S., B., K. 2011, Influence of dynamic sodium environment on the creep-fatigue behavior of Modified 9Cr-1Mo ferritic-martensitic steel, Nuclear Engineering and Design, Vol.241, pp.2807-281
- Kannan, R., Sandhya, R., Ganesan, V., Valsan, M., Rao, S., B., K. 2009, Effect of sodium environment on the low cycle fatigue properties of modified 9Cr-1Mo ferritic martensitic steel, Journal of Nuclear Materials, Vol.384, pp.286-291
- Kasahara, N., 2001, Strain concentration at structural discontinuities and its prediction based on characteristics of compliance change in structure, JSME International Journal Series A Vol.44, No.3 pp.354-361, 2001
- Kurome, K., Murakami, H., Tsujita, Y., Futagami, S., Hayafune, H., Development of the main components for JSFR, Proceedings of 2010 International Congress on Advances in Nuclear Power Plants (ICAPP '10), 2010, pp.637-644
- Miyahara, M., and Tokimasa, K., 1995, Relationship between creep-fatigue damage rule based on strain range partitioning concept and small crack growth behavior, Journal society of material science Japan, Vol.44, pp.71-77, (Japanese)

Table list

Table 1 Material properties used for the FEA

Temperature (℃)	Young's modulus (N/mm^2)	Poisson's ratio	Instantaneous coefficient of thermal expansion ($10^{-6}mm/mm/℃$)	Thermal conductivity (W/m·K)	Specific heat (J/g·K)	Proportional limit (N/mm^2)	Work hardening coefficient (N/mm^2)
250	202800	0.300	12.21	26.95	0.522	331	20106
275	201100	0.300	12.37	27.27	0.535	331	20106
300	199300	0.300	12.53	27.50	0.547	331	20106
325	197300	0.300	12.68	27.66	0.559	331	20106
350	195300	0.300	12.83	27.77	0.572	331	20106
375	193000	0.300	12.98	27.80	0.584	321	20333
400	191000	0.300	13.12	27.95	0.601	310	20439
425	189000	0.300	13.25	27.95	0.618	297	20408
450	186000	0.300	13.38	28.09	0.642	283	20226
475	183000	0.301	13.51	27.99	0.659	268	19879
500	181000	0.302	13.63	27.95	0.681	252	19361
525	178000	0.304	13.75	27.95	0.704	235	18667
550	175000	0.306	13.86	27.87	0.731	217	17801
575	172000	0.308	13.97	27.77	0.762	199	16771
600	169000	0.310	14.07	27.73	0.794	181	15593
625	166000	0.312	14.17	27.66	0.826	164	14287
650	163000	0.314	14.27	27.59	0.862	148	12878

Figure list

Fig1

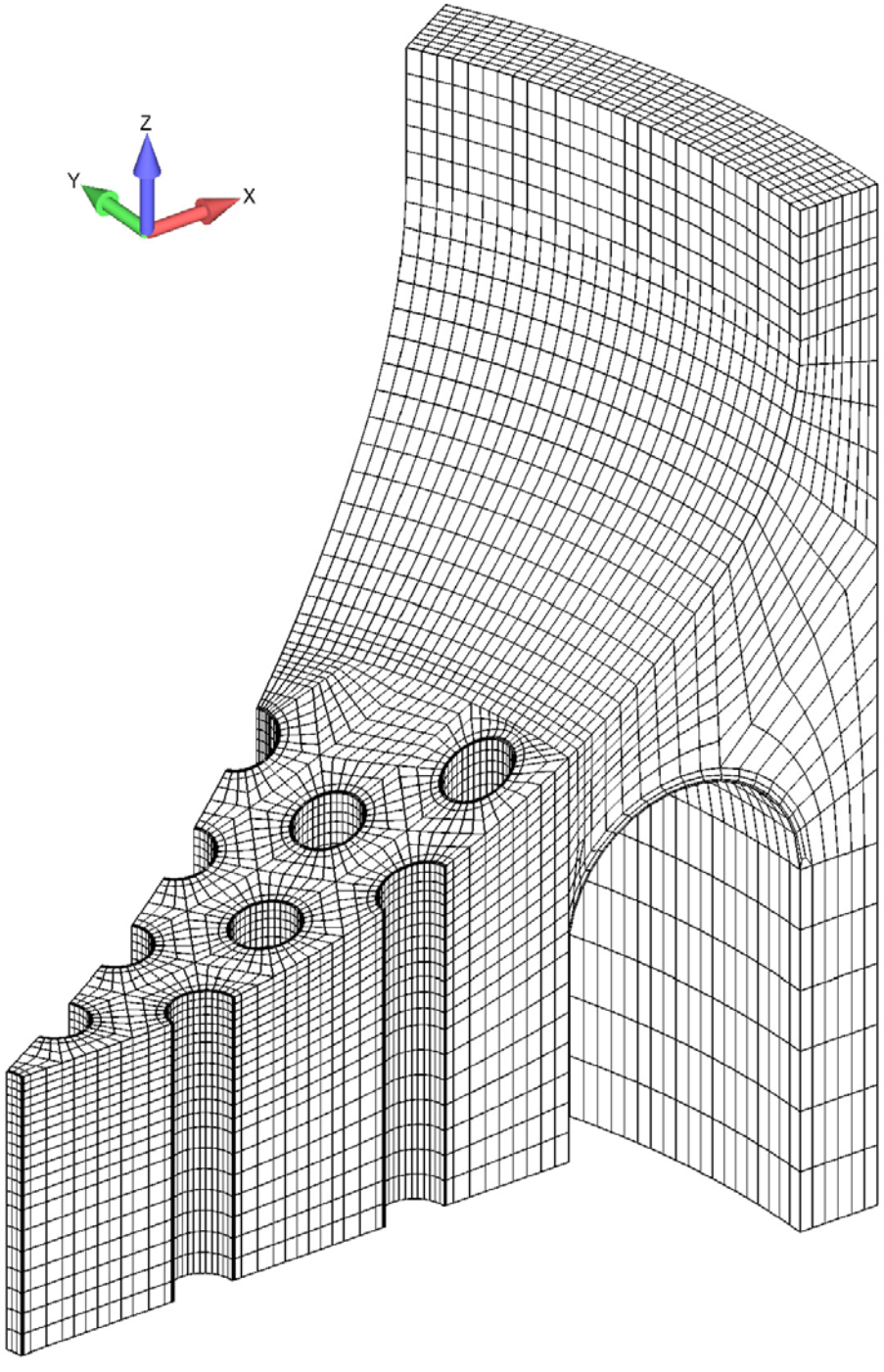

Fig.2

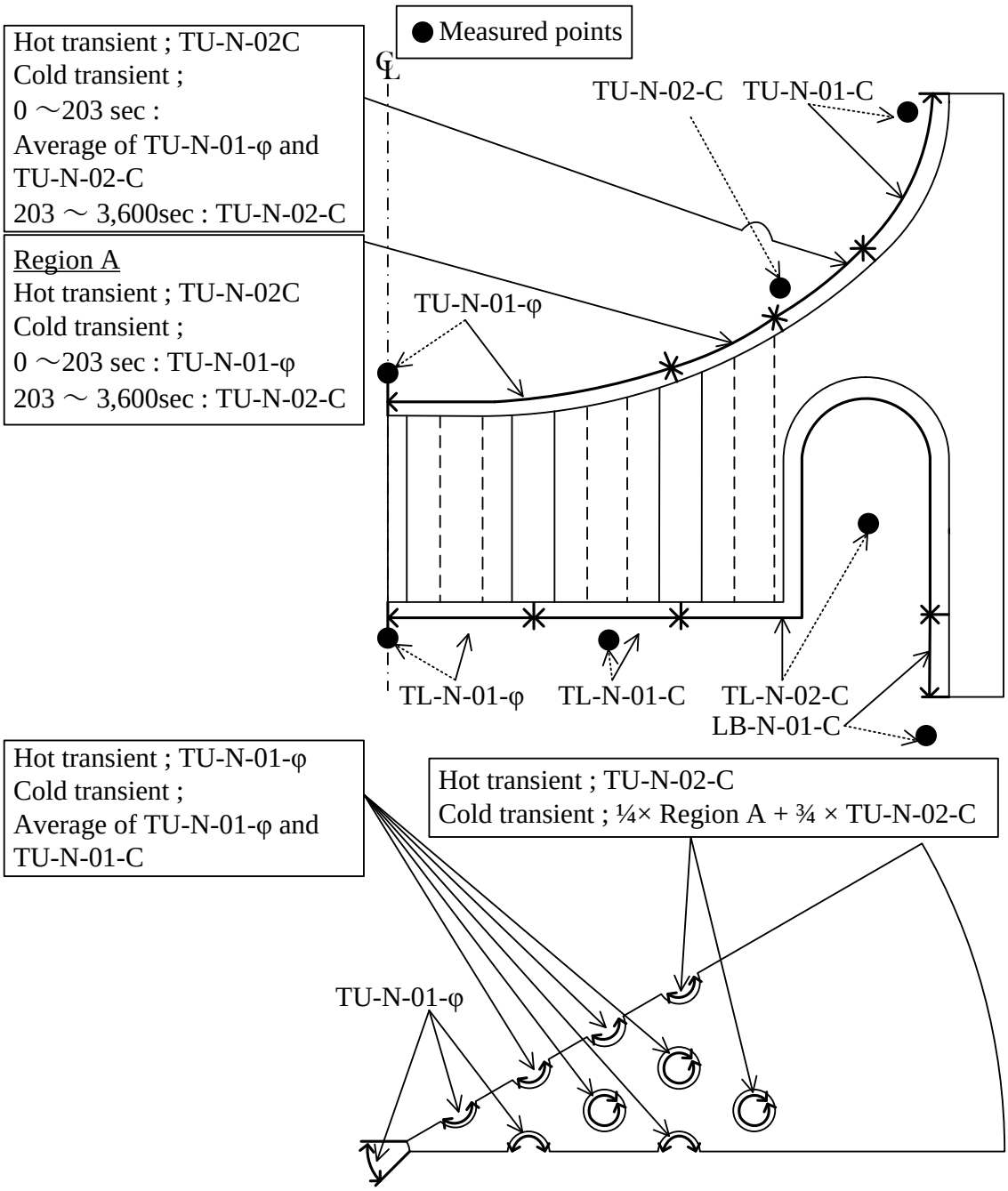
Measured points
Hot transient ; TU-N-02C
Cold transient ;
0 ～203 sec :
Average of TU-N-01-φ and TU-N-02-C
203 ～ 3,600sec : TU-N-02-C
Region A
Hot transient ; TU-N-02C
Cold transient ;
0 ～203 sec : TU-N-01-φ
203 ～ 3,600sec : TU-N-02-C
CL
TU-N-02-C
TU-N-01-C
TU-N-01-φ
TL-N-01-φ
TL-N-01-C
TL-N-02-C
LB-N-01-C
Hot transient ; TU-N-01-φ
Cold transient ;
Average of TU-N-01-φ and TU-N-01-C
Hot transient ; TU-N-02-C
Cold transient ; ¼× Region A + ¾ × TU-N-02-C
TU-N-01-φ

Fig.3

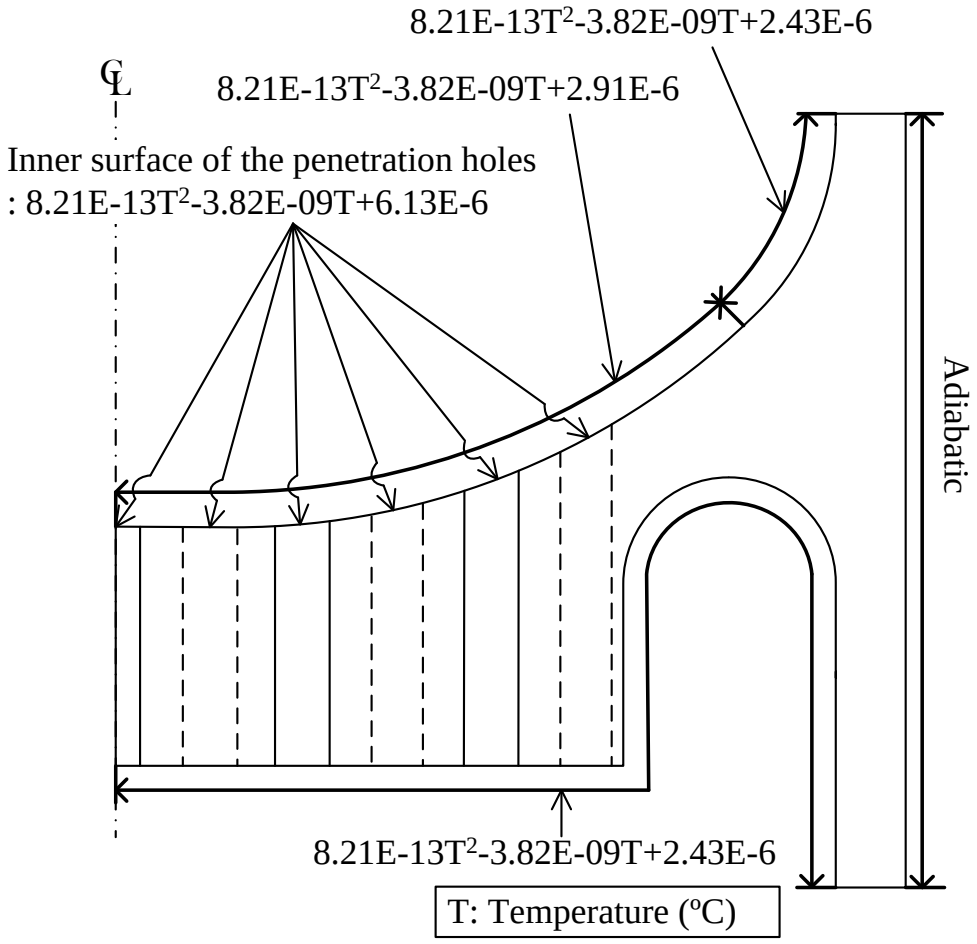
8.21E-13T2-3.82E-09T+2.43E-6
CL
8.21E-13T2-3.82E-09T+2.91E-6
Inner surface of the penetration holes
: 8.21E-13T2-3.82E-09T+6.13E-6
Adiabatic
8.21E-13T2-3.82E-09T+2.43E-6
T: Temperature (ºC)

Fig.4

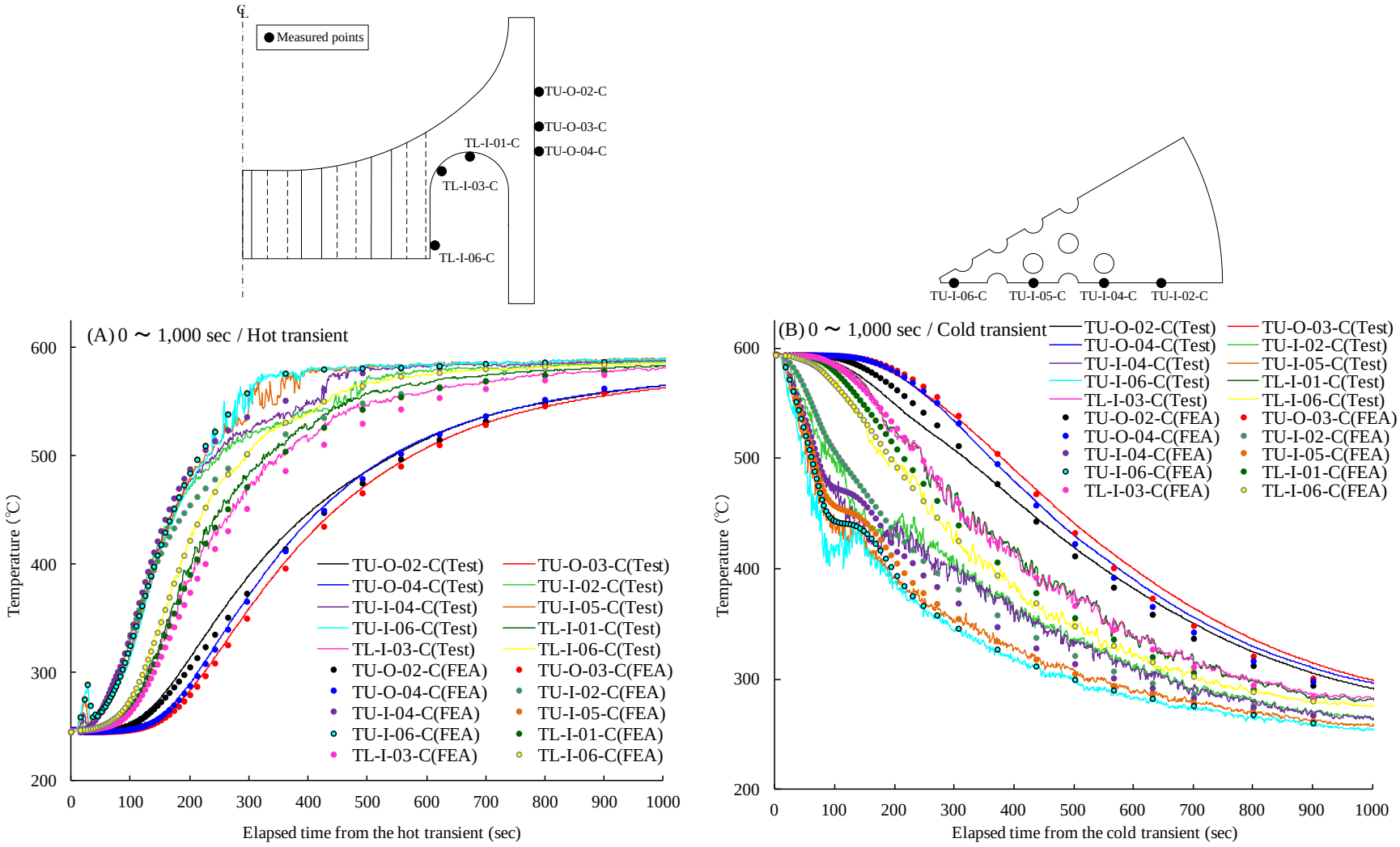
Measured points
TU-O-02-C
TU-O-03-C
TU-O-04-C
TL-I-01-C
TL-I-03-C
TL-I-06-C
TU-I-06-C
TU-I-05-C
TU-I-04-C
TU-I-02-C
(A) 0 ~ 1,000 sec / Hot transient
Temperature (℃)
Elapsed time from the hot transient (sec)
(B) 0 ~ 1,000 sec / Cold transient
Elapsed time from the cold transient (sec)
TU-O-02-C(Test)
TU-O-03-C(Test)
TU-O-04-C(Test)
TU-I-02-C(Test)
TU-I-04-C(Test)
TU-I-05-C(Test)
TU-I-06-C(Test)
TL-I-01-C(Test)
TL-I-03-C(Test)
TL-I-06-C(Test)
TU-O-02-C(FEA)
TU-O-03-C(FEA)
TU-O-04-C(FEA)
TU-I-02-C(FEA)
TU-I-04-C(FEA)
TU-I-05-C(FEA)
TU-I-06-C(FEA)
TL-I-01-C(FEA)
TL-I-03-C(FEA)
TL-I-06-C(FEA)

Fig.5

(A)182 sec from the hot transient

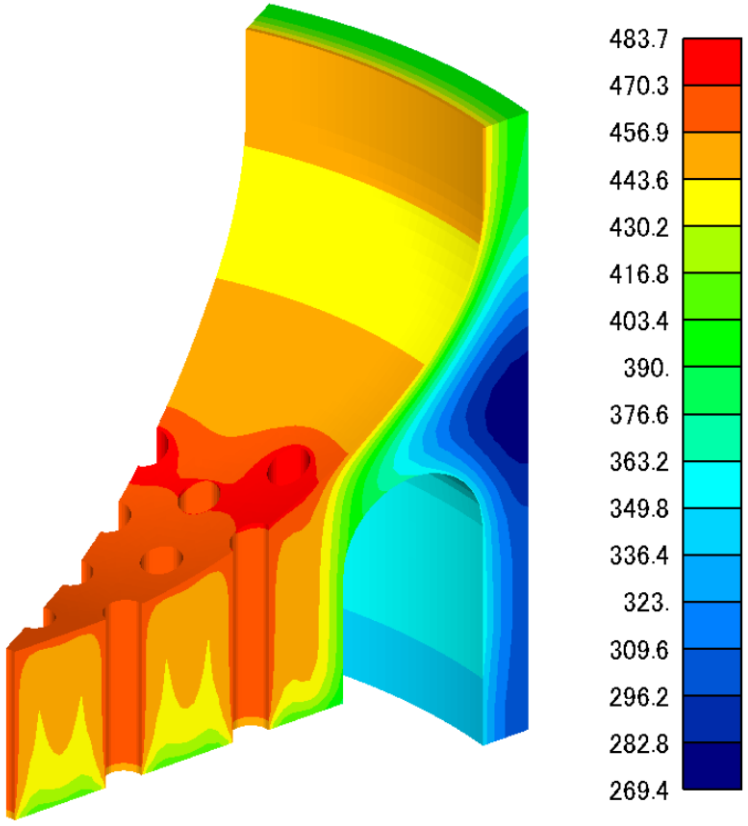

(B)110 sec from the cold transient

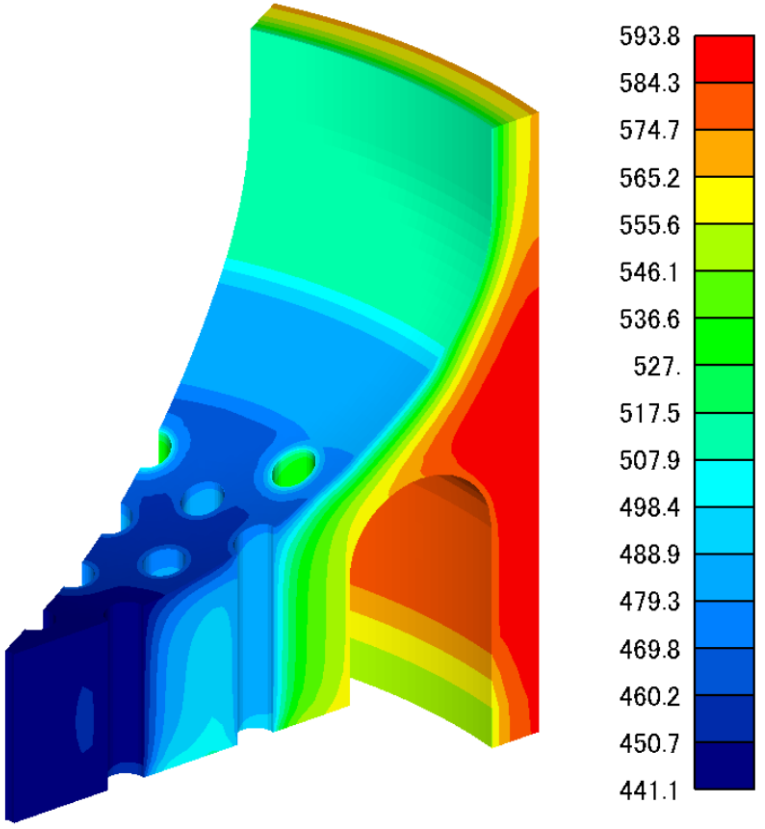

Fig.6

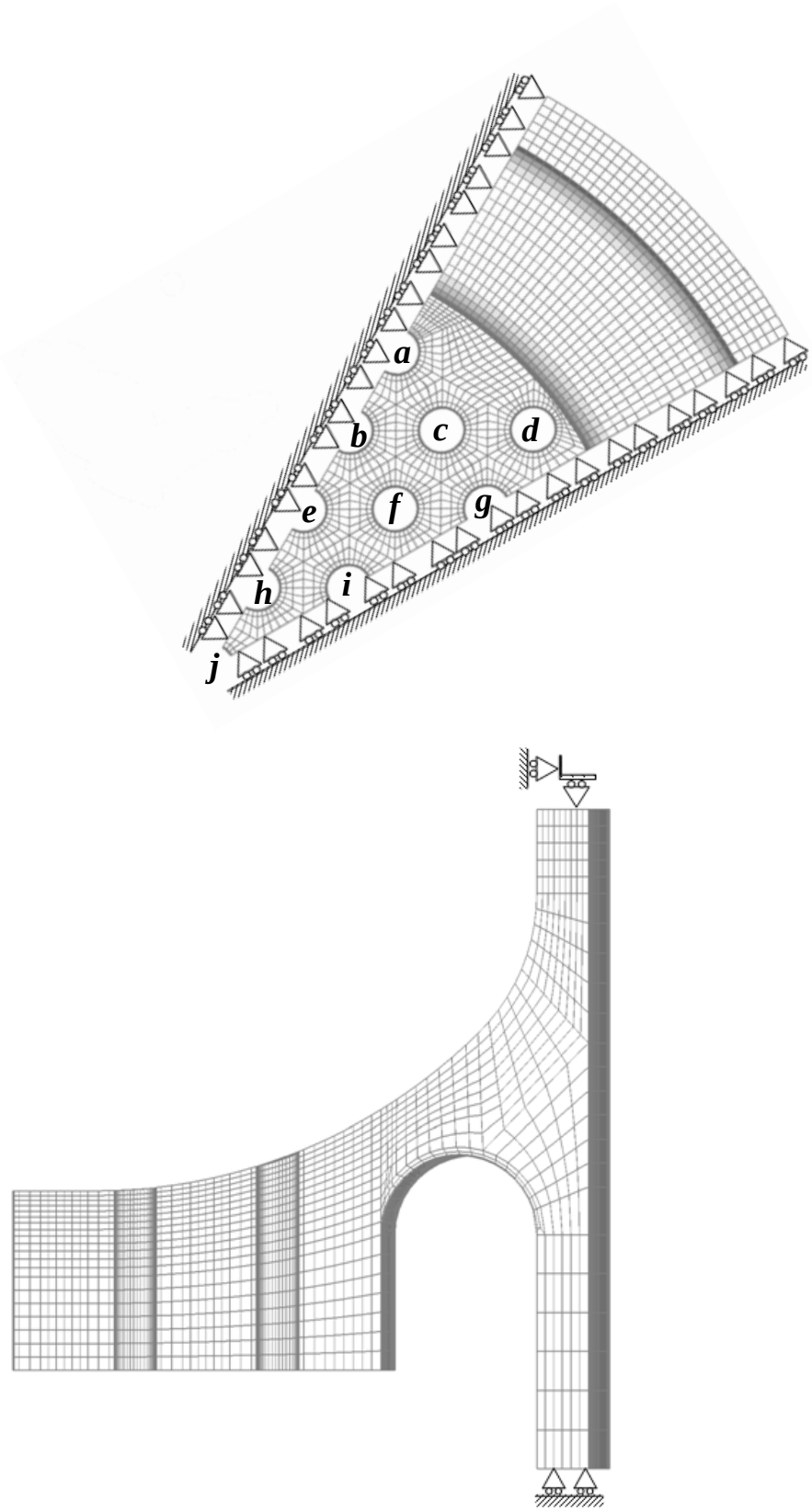

Fig.7

(A)182 sec in the hot transient

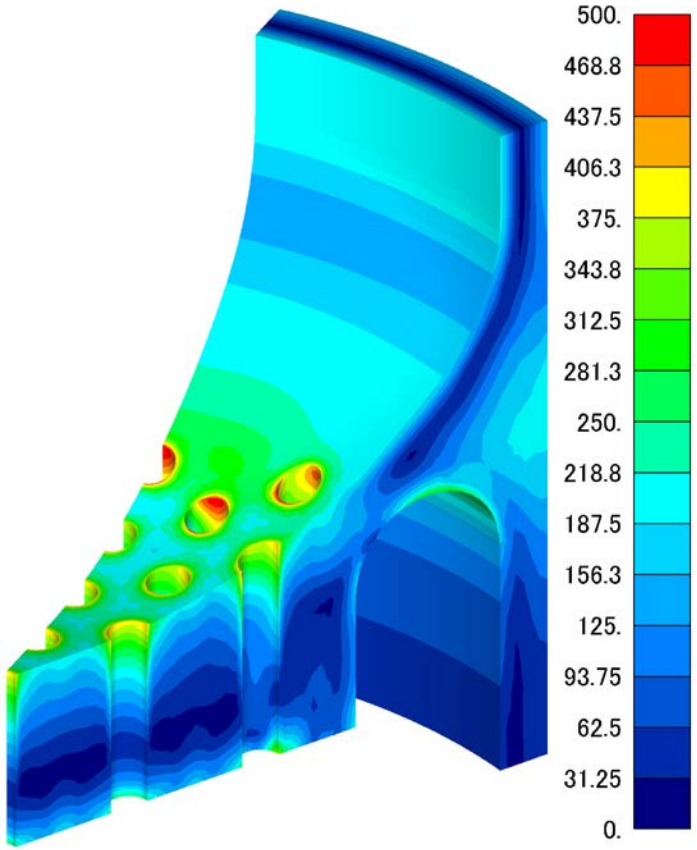

(B)110 sec in the cold transient

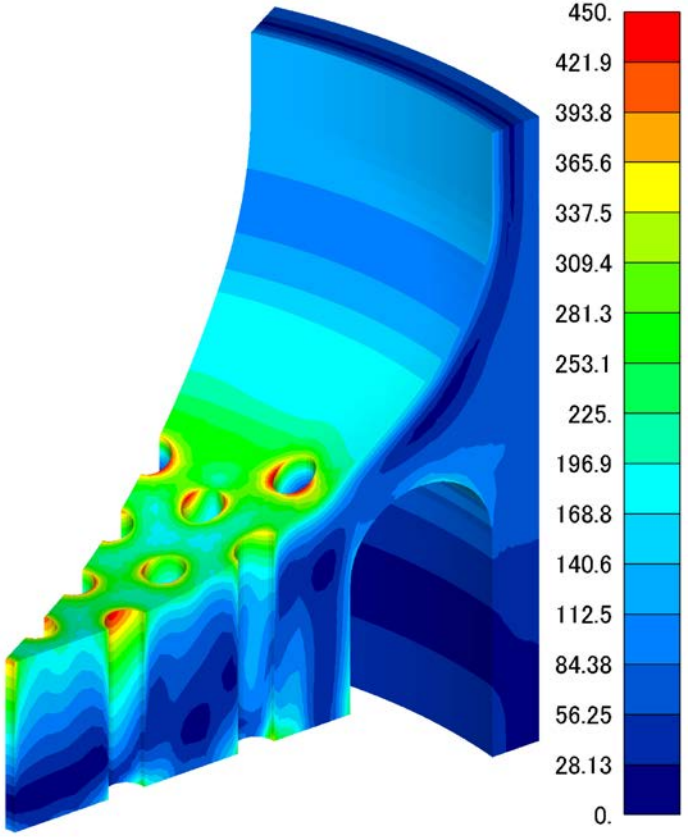

Fig.8

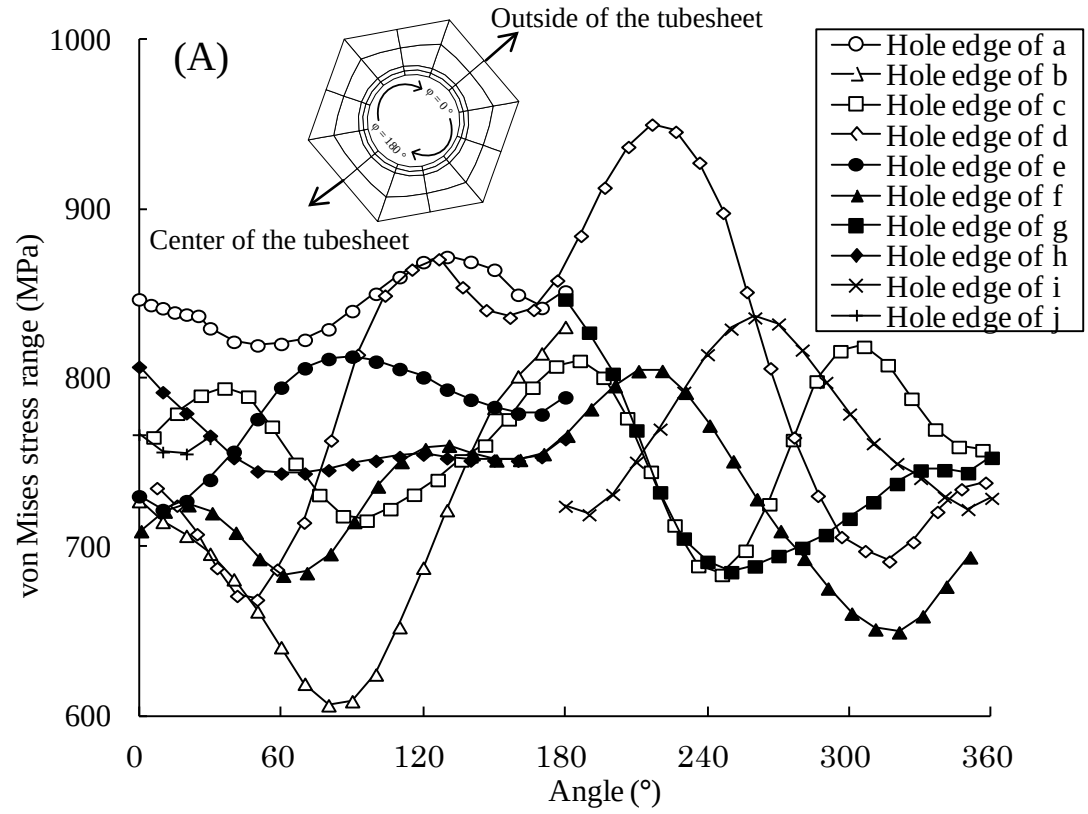
(A)
Outside of the tubesheet
Center of the tubesheet
φ = 0°
φ = 180°
Hole edge of a
Hole edge of b
Hole edge of c
Hole edge of d
Hole edge of e
Hole edge of f
Hole edge of g
Hole edge of h
Hole edge of i
Hole edge of j
von Mises stress range (MPa)
1000
900
800
700
600
0
60
120
180
240
300
360
Angle (°)

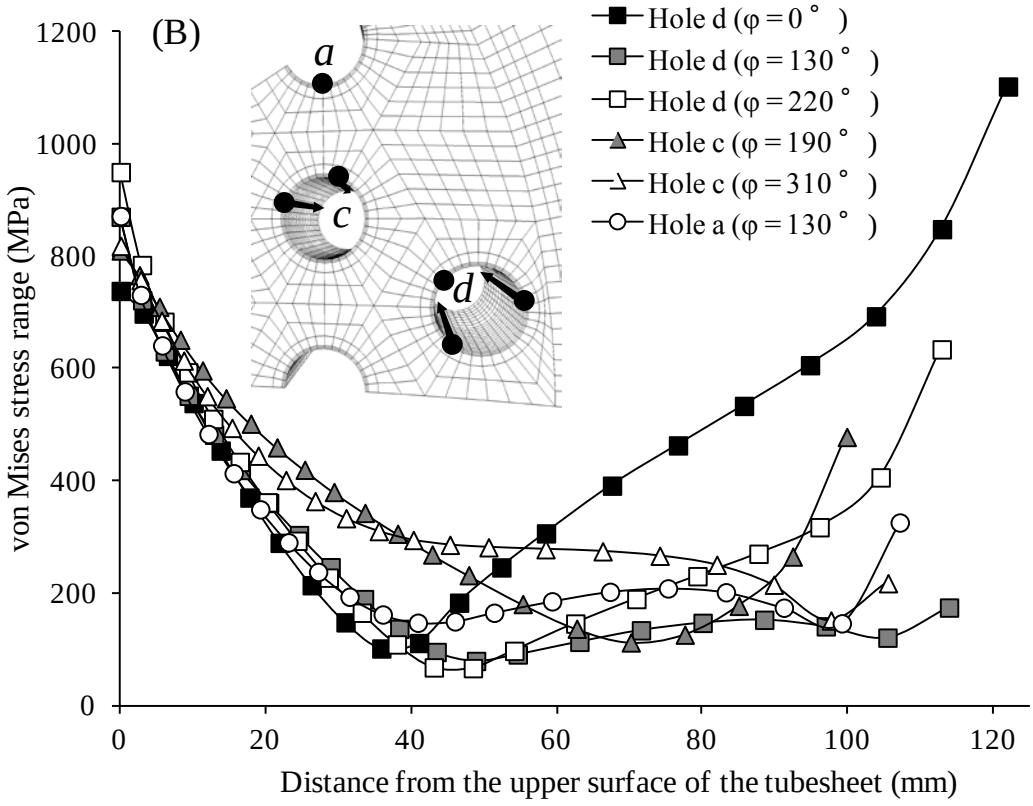
(B)
a
c
d
Hole d (φ = 0 °)
Hole d (φ = 130 °)
Hole d (φ = 220 °)
Hole c (φ = 190 °)
Hole c (φ = 310 °)
Hole a (φ = 130 °)
von Mises stress range (MPa)
1200
1000
800
600
400
200
0
0
20
40
60
80
100
120
Distance from the upper surface of the tubesheet (mm)

Fig.9

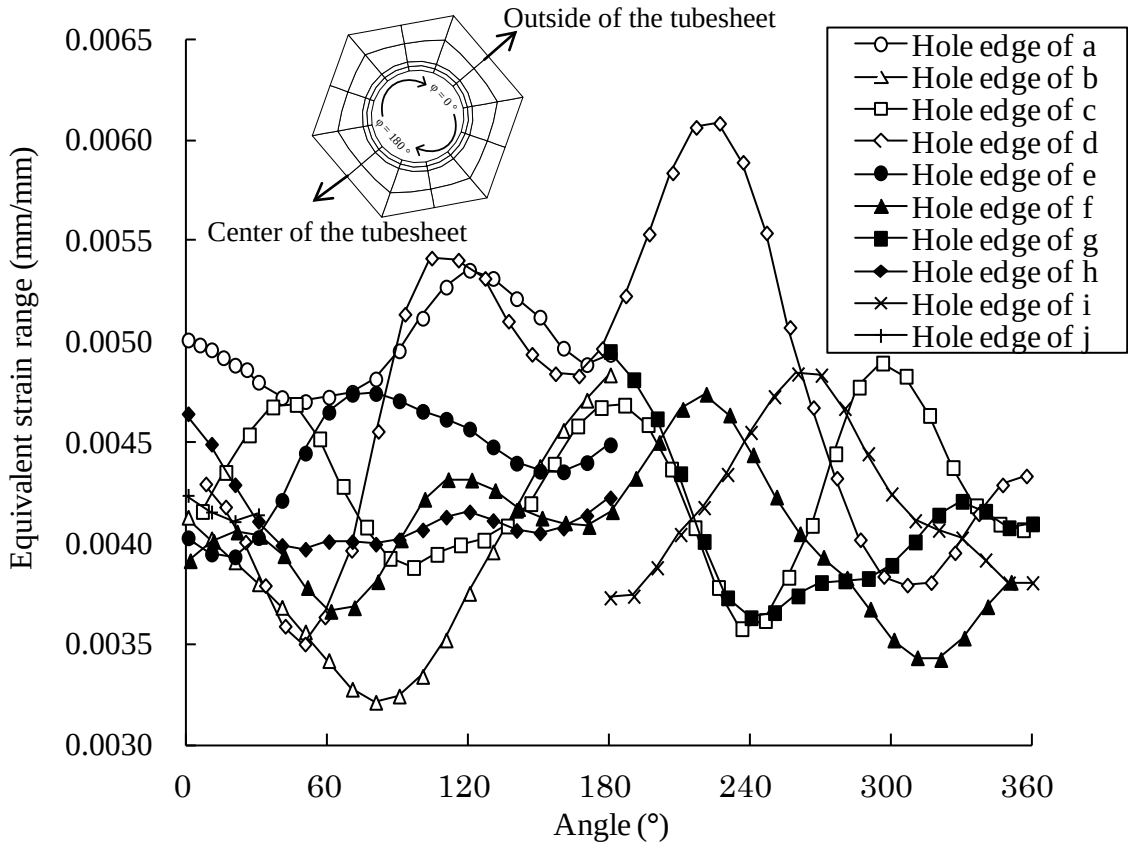
Outside of the tubesheet
Center of the tubesheet
φ = 0°
φ = 180°
Hole edge of a
Hole edge of b
Hole edge of c
Hole edge of d
Hole edge of e
Hole edge of f
Hole edge of g
Hole edge of h
Hole edge of i
Hole edge of j
Equivalent strain range (mm/mm)
0.0065
0.0060
0.0055
0.0050
0.0045
0.0040
0.0035
0.0030
0
60
120
180
240
300
360
Angle (°)

Fig.10

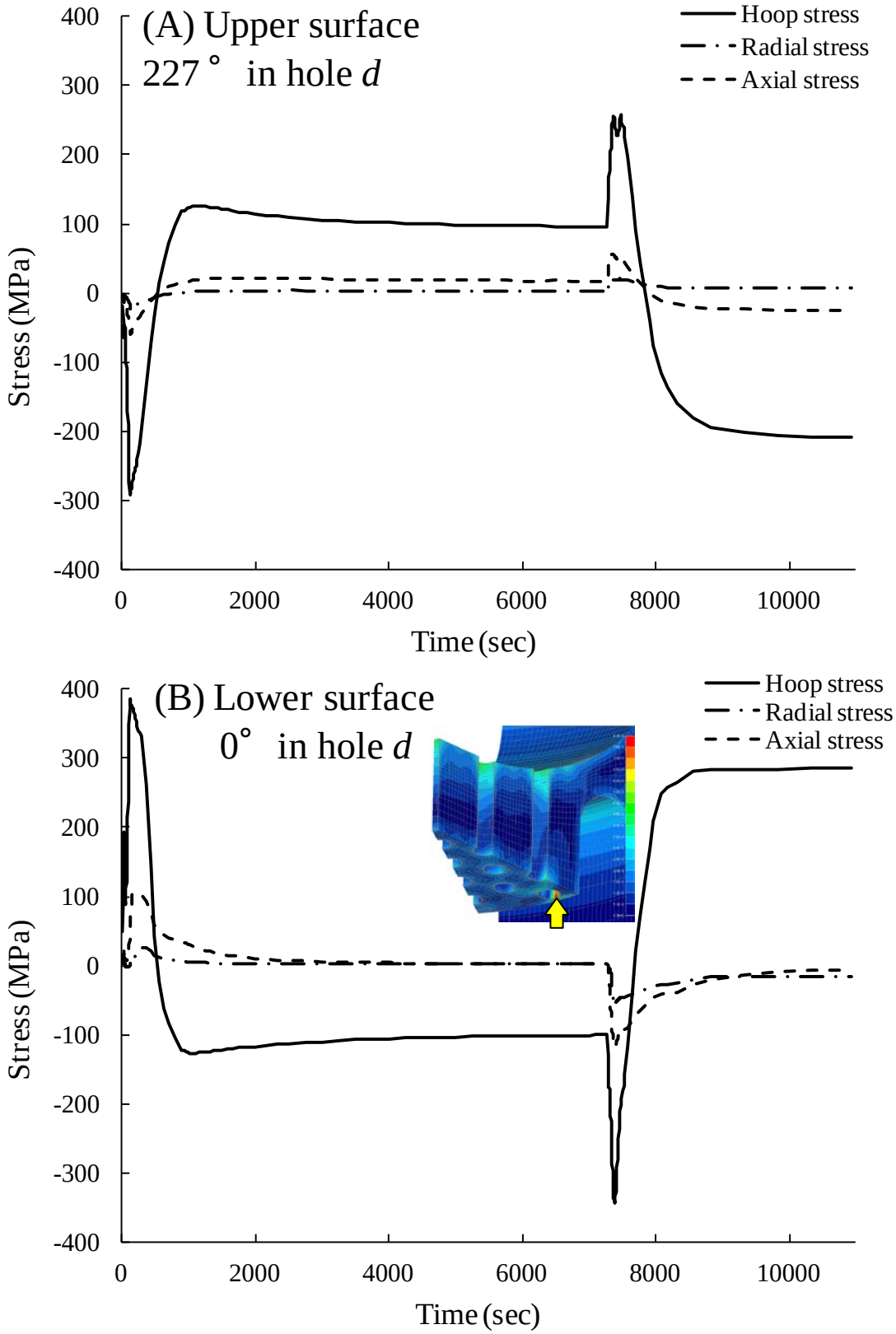
(A) Upper surface
227 ° in hole d
Hoop stress
Radial stress
Axial stress
Stress (MPa)
Time (sec)
400
300
200
100
0
-100
-200
-300
-400
0
2000
4000
6000
8000
10000
(B) Lower surface
0° in hole d
Hoop stress
Radial stress
Axial stress
Stress (MPa)
Time (sec)

Fig.11

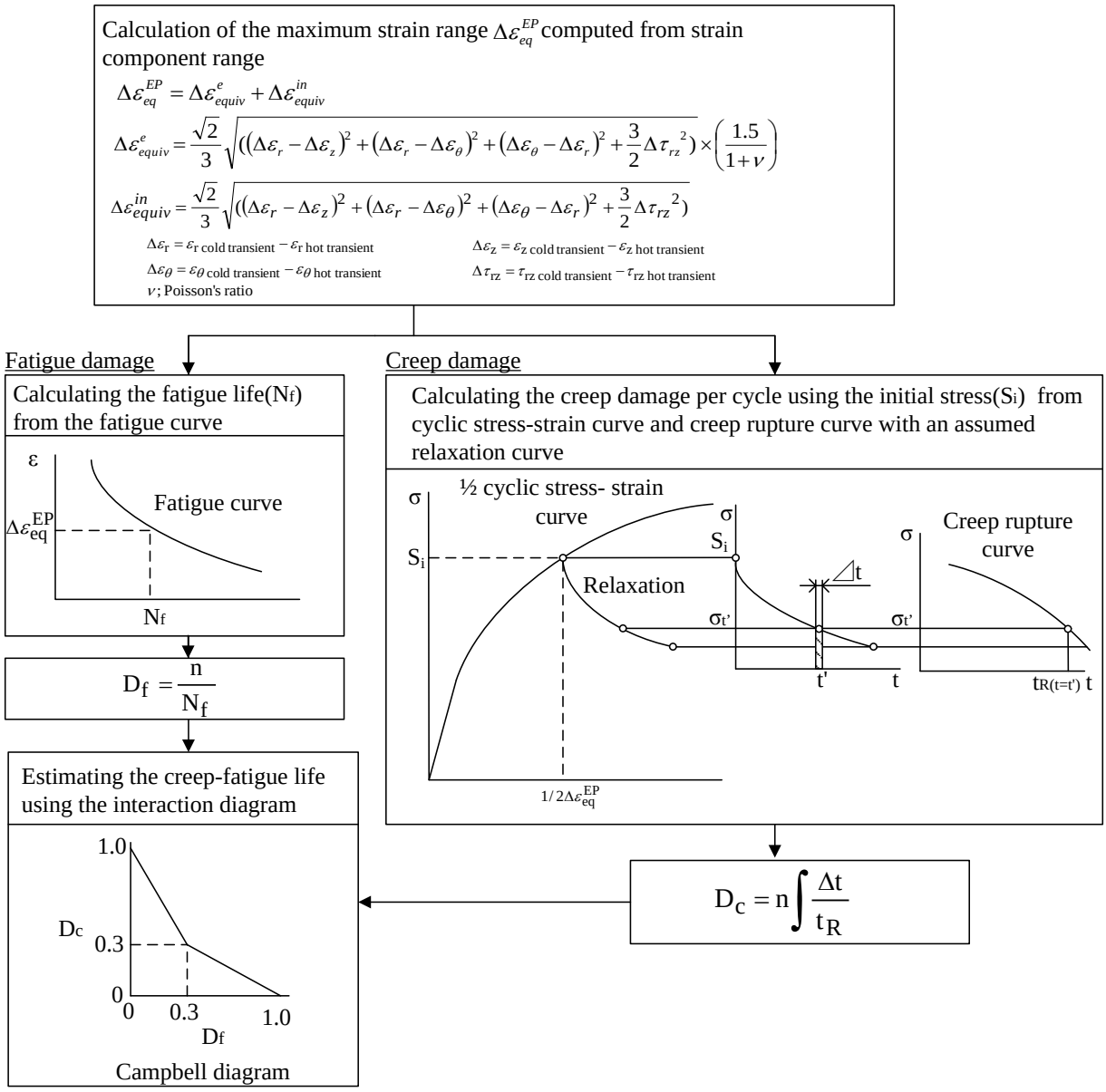
Calculation of the maximum strain range $\Delta\varepsilon_{eq}^{EP}$ computed from strain component range
$\Delta\varepsilon_{eq}^{EP} = \Delta\varepsilon_{equiv}^{e} + \Delta\varepsilon_{equiv}^{in}$
$\Delta\varepsilon_{equiv}^{e} = \frac{\sqrt{2}}{3}\sqrt{((\Delta\varepsilon_r - \Delta\varepsilon_z)^2 + (\Delta\varepsilon_r - \Delta\varepsilon_\theta)^2 + (\Delta\varepsilon_\theta - \Delta\varepsilon_r)^2 + \frac{3}{2}\Delta\tau_{rz}{}^2)} \times \left(\frac{1.5}{1+\nu}\right)$
$\Delta\varepsilon_{equiv}^{in} = \frac{\sqrt{2}}{3}\sqrt{((\Delta\varepsilon_r - \Delta\varepsilon_z)^2 + (\Delta\varepsilon_r - \Delta\varepsilon_\theta)^2 + (\Delta\varepsilon_\theta - \Delta\varepsilon_r)^2 + \frac{3}{2}\Delta\tau_{rz}{}^2)}$
$\Delta\varepsilon_r = \varepsilon_r$ cold transient $- \varepsilon_r$ hot transient
$\Delta\varepsilon_z = \varepsilon_z$ cold transient $- \varepsilon_z$ hot transient
$\Delta\varepsilon_\theta = \varepsilon_\theta$ cold transient $- \varepsilon_\theta$ hot transient
$\Delta\tau_{rz} = \tau_{rz}$ cold transient $- \tau_{rz}$ hot transient
ν; Poisson's ratio
Fatigue damage
Creep damage
Calculating the fatigue life(N_f) from the fatigue curve
ε
Fatigue curve
$\Delta\varepsilon_{eq}^{EP}$
N_f
$D_f = \frac{n}{N_f}$
Calculating the creep damage per cycle using the initial stress(S_i) from cyclic stress-strain curve and creep rupture curve with an assumed relaxation curve
σ
½ cyclic stress- strain curve
S_i
Relaxation
$\sigma_{t'}$
Δt
t'
t
Creep rupture curve
$t_{R(t=t')}$
$1/2\Delta\varepsilon_{eq}^{EP}$
$D_c = n\int \frac{\Delta t}{t_R}$
Estimating the creep-fatigue life using the interaction diagram
1.0
D_c
0.3
0
0
0.3
1.0
D_f
Campbell diagram

Fig.12

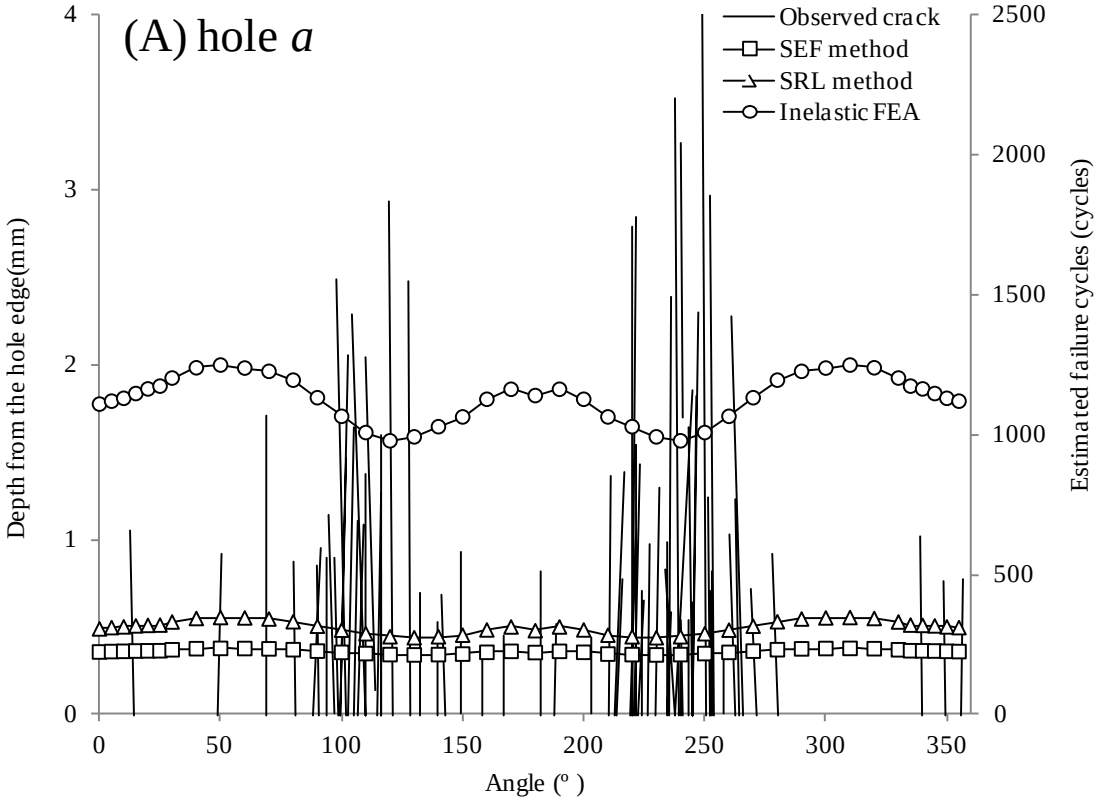
(A) hole *a*
Observed crack
SEF method
SRL method
Inelastic FEA
Depth from the hole edge(mm)
Estimated failure cycles (cycles)
Angle (º)
0
1
2
3
4
0
500
1000
1500
2000
2500
0
50
100
150
200
250
300
350

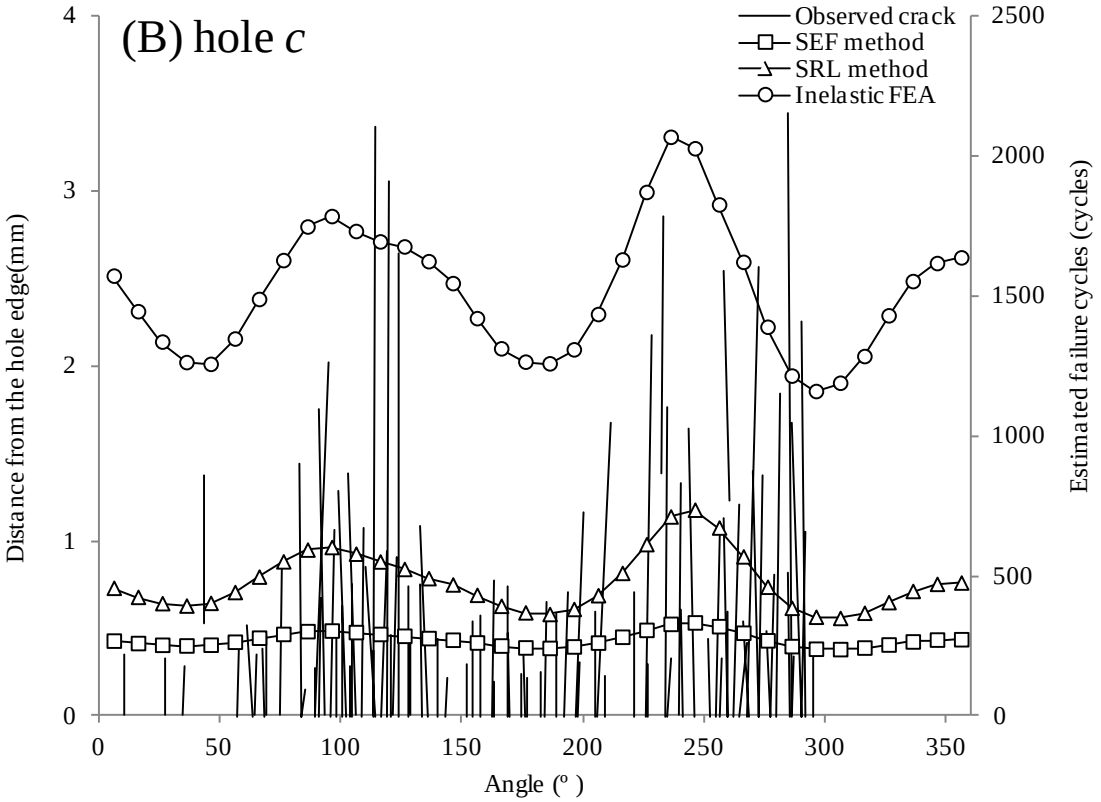
(B) hole *c*
Observed crack
SEF method
SRL method
Inelastic FEA
Distance from the hole edge(mm)
Estimated failure cycles (cycles)
Angle (º)
0
1
2
3
4
0
500
1000
1500
2000
2500
0
50
100
150
200
250
300
350

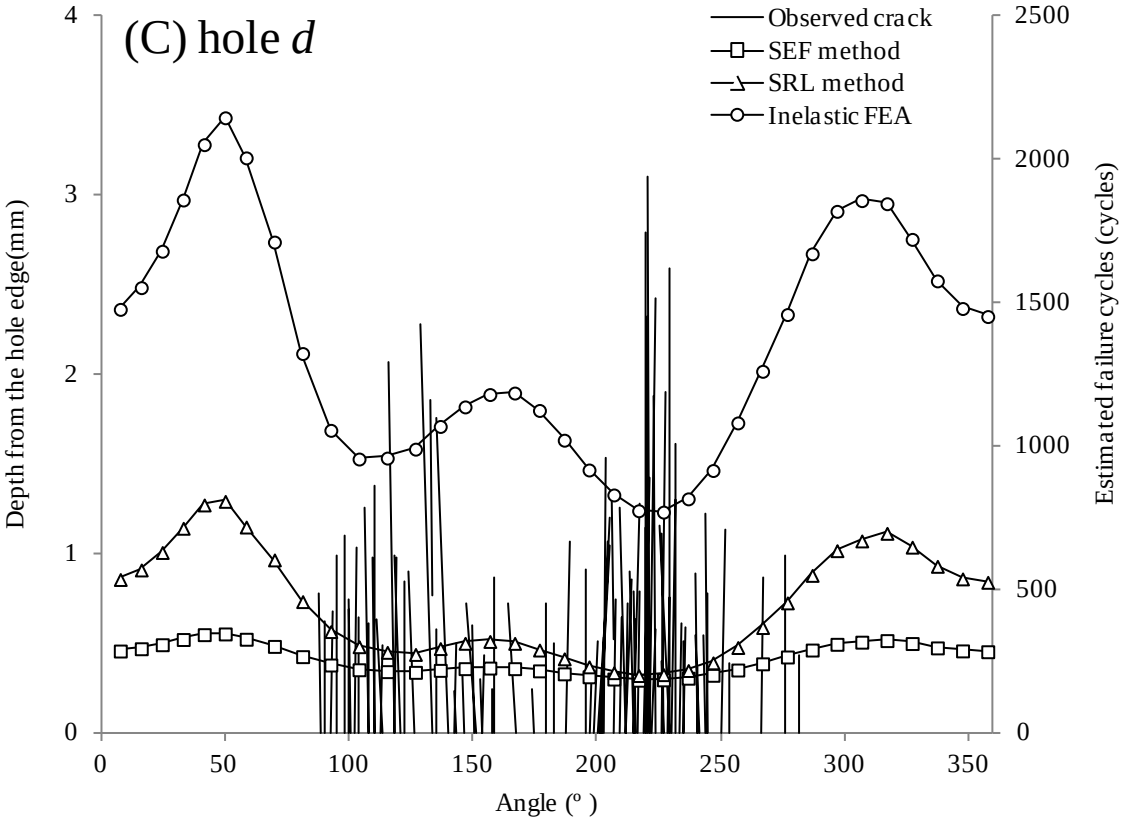
(C) hole *d*
Observed crack
SEF method
SRL method
Inelastic FEA
Depth from the hole edge(mm)
Estimated failure cycles (cycles)
Angle (º)
0
1
2
3
4
0
500
1000
1500
2000
2500
0
50
100
150
200
250
300
350

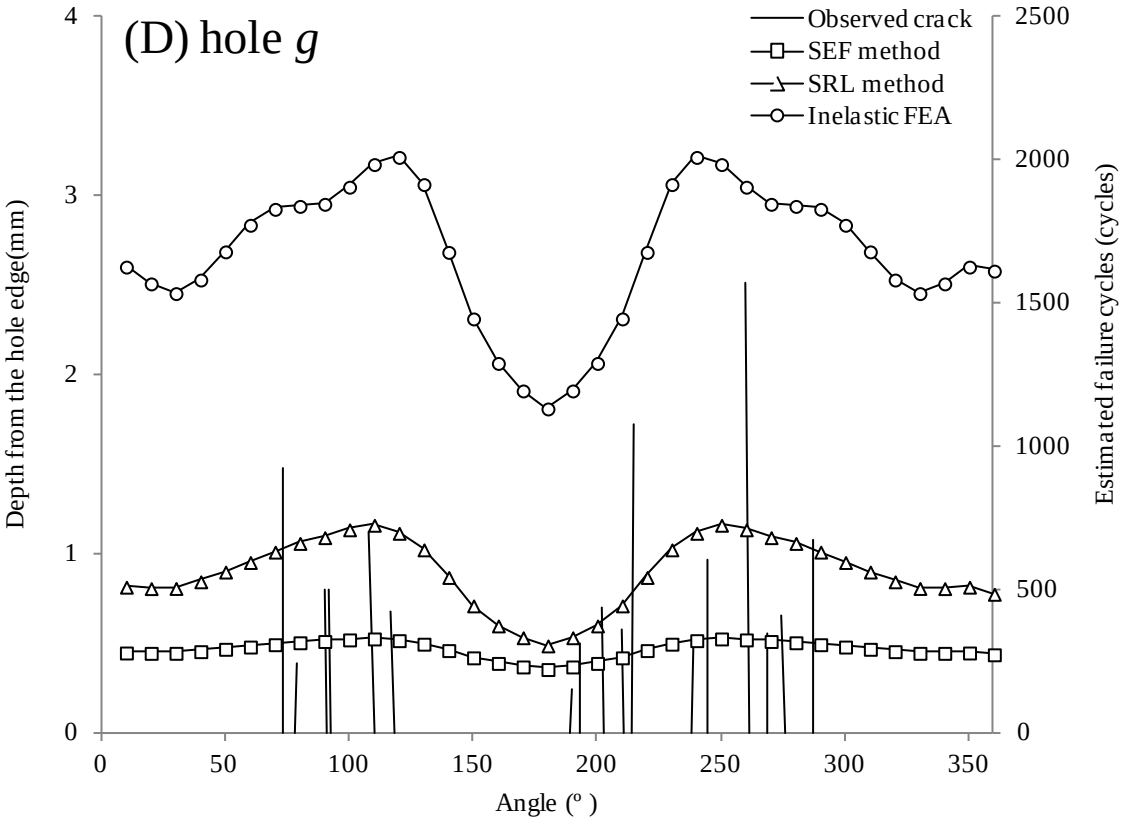
(D) hole *g*
Observed crack
SEF method
SRL method
Inelastic FEA
Depth from the hole edge(mm)
Estimated failure cycles (cycles)
Angle (º)
0
1
2
3
4
0
500
1000
1500
2000
2500
0
50
100
150
200
250
300
350

Fig.13

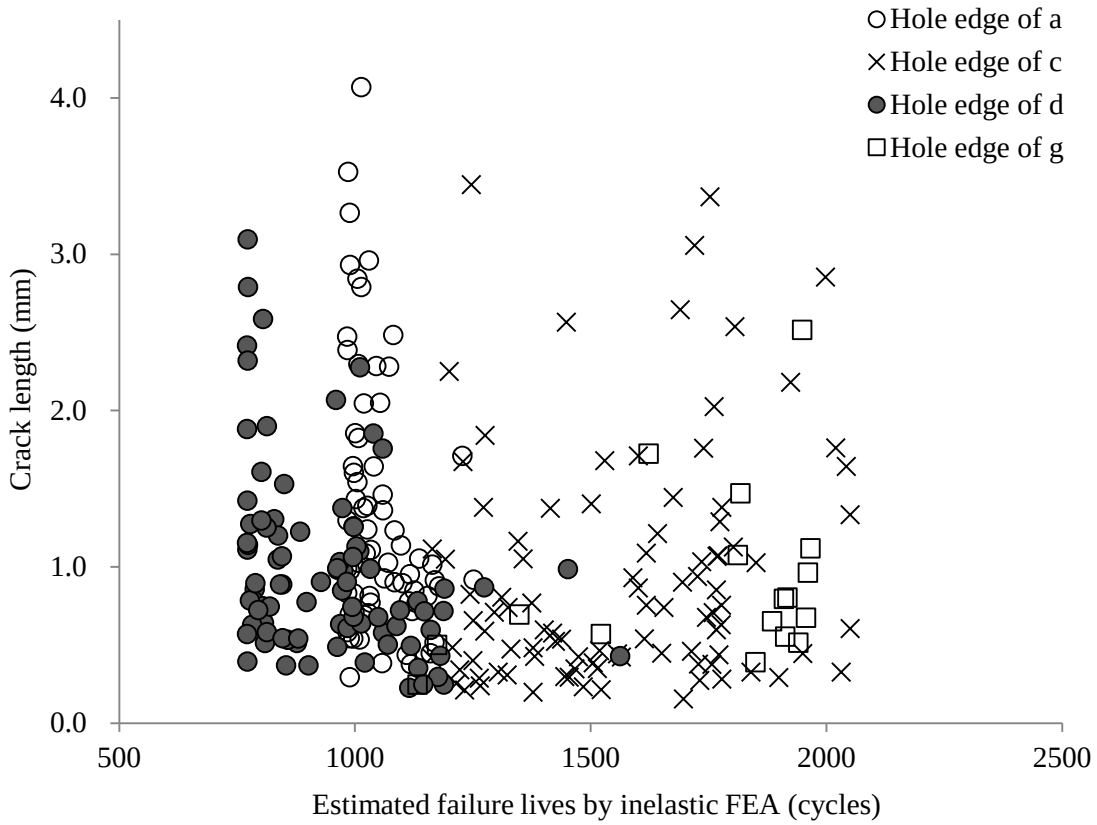
Hole edge of a
Hole edge of c
Hole edge of d
Hole edge of g
Crack length (mm)
4.0
3.0
2.0
1.0
0.0
500
1000
1500
2000
2500
Estimated failure lives by inelastic FEA (cycles)

Fig.14

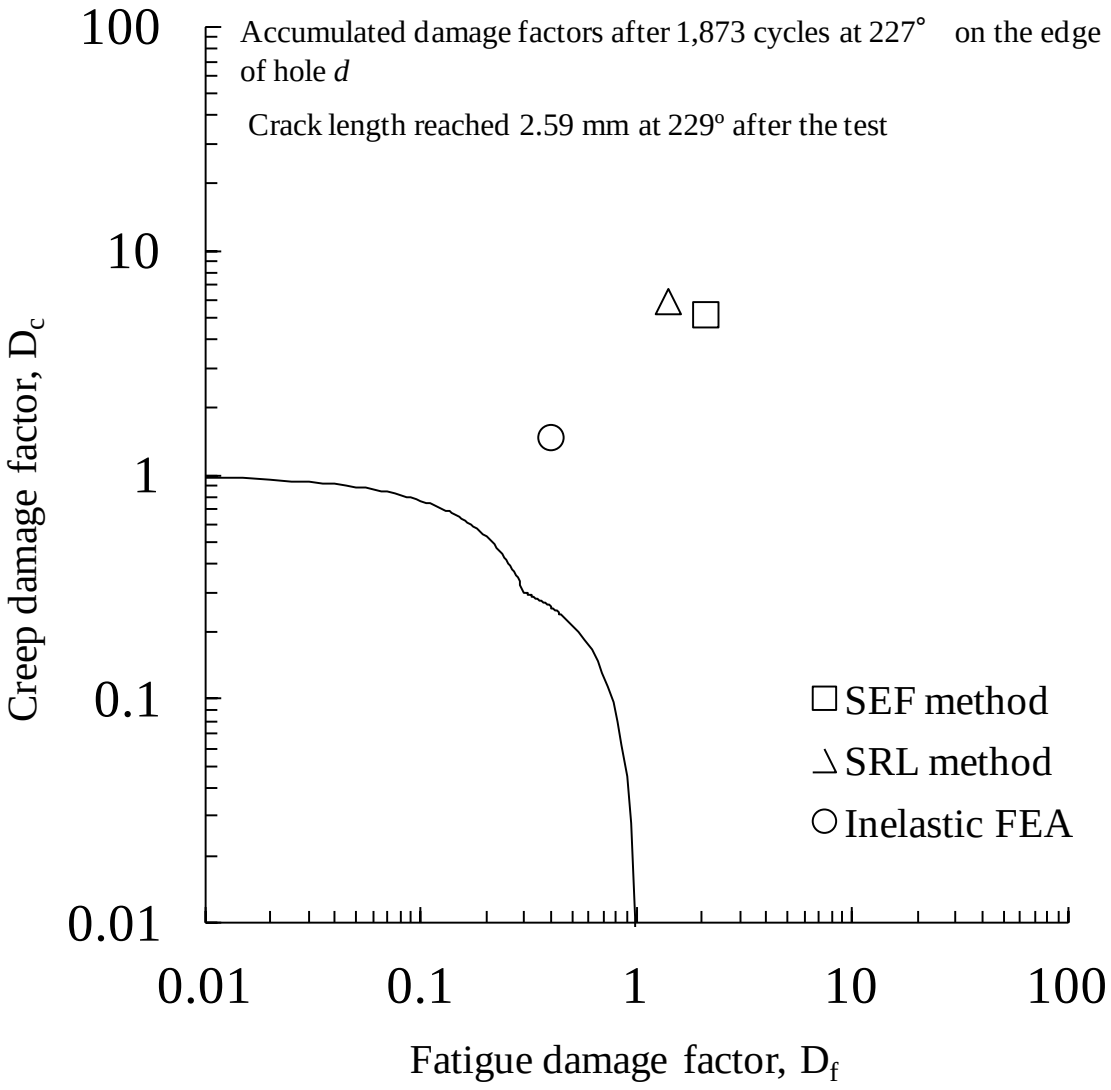
Accumulated damage factors after 1,873 cycles at 227° on the edge of hole *d*
Crack length reached 2.59 mm at 229° after the test
100
10
1
0.1
0.01
Creep damage factor, D_c
0.01
0.1
1
10
100
Fatigue damage factor, D_f
SEF method
SRL method
Inelastic FEA

Fig.15

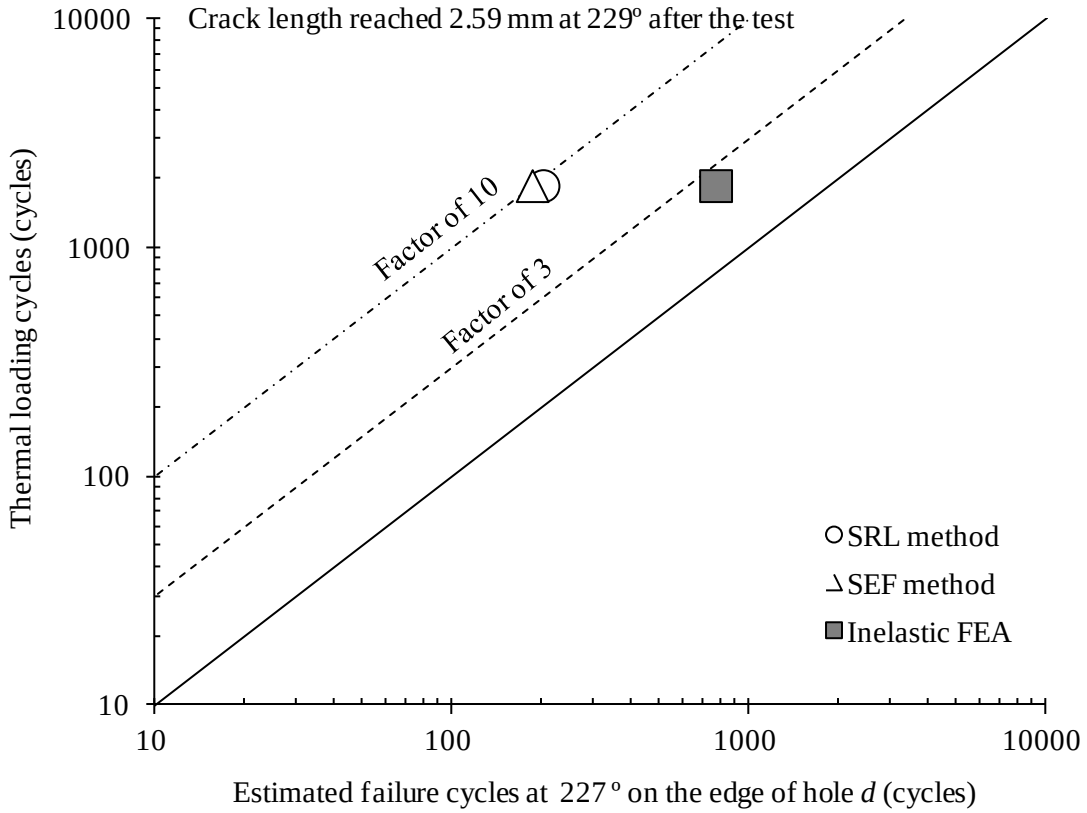
Crack length reached 2.59 mm at 229º after the test
Factor of 10
Factor of 3
SRL method
SEF method
Inelastic FEA
Thermal loading cycles (cycles)
Estimated failure cycles at 227 º on the edge of hole d (cycles)
10000
1000
100
10
10
100
1000
10000